MNRAS **000**, 1–11 (2016) Preprint 6 June 2016 Compiled using MNRAS LATEX style file v3.0

Recent X-ray observations of the symbiotic star AG Peg: do they signify Colliding Stellar Winds?

Svetozar A. Zhekov[1⋆] and Toma Tomov[2]
[1] *Institute of Astronomy and National Astronomical Observatory, 72 Tsarigradsko Chaussee Blvd., Sofia 1784, Bulgaria*
[2] *Centre for Astronomy, Faculty of Physics, Astronomy and Informatics, Nicolaus Copernicus University, Grudziadzka 5, 87-100 Torun, Poland*

arXiv:1606.01201v1 [astro-ph.SR] 3 Jun 2016

ABSTRACT

We present an analysis of recent X-ray observations of the symbiotic star AG Peg. The X-ray emission of AG Peg as observed with *Swift* in 2015 shows considerable variability on time scale of days as variability on shorter time scales might be present as well. Analysis of the X-ray spectra obtained in 2013 and 2015 confirms that AG Peg is an X-ray source of class β of the X-ray sources amongst the symbiotic stars. The X-ray emission of AG Peg as observed with *ROSAT* (1993 June) might well originate from colliding stellar winds (CSW) in binary system. On the other hand, the characteristics of the X-ray emission of AG Peg in 2013 and 2015 (*Swift*) are hard to accommodate in the framework of the CSW picture. Analysis of the light curves in 2015 shows that the power spectrum of the X-ray variability in AG Peg resembles that of the flicker noise (or flickering) being typical for accretion processes in astronomical objects. This is a sign that CSWs did not play a key role for the X-ray emission from AG Peg in 2013-2015 and a different mechanism (probably accretion) is also getting into play.

Key words: shock waves – stars: individual: AG Peg – stars: binaries: symbiotic – X-rays: stars.

1 INTRODUCTION

AG Peg (HD 207757) is an old symbiotic nova whose outburst occurred in the mid-19th century and was characterized with a slow rise to its maximum and a slower decline (lasting for many decades). This is likely the slowest classical nova eruption amongst recorded until present day (e.g., Kenyon et al. 1993; Kenyon, Proga & Keyes 2001 and references therein). Recently, there were reports about ongoing changes of the AG Peg emission in the optical (Munari et al. 2013) and in the X-rays (Nunez & Luna 2013; Luna et al. 2015; Ramsay et al. 2015). This gives solid indications about a new type of activity in the evolution of this old symbiotic nova.

AG Peg was first detected in X-rays with *ROSAT* (Mürset, Jordan & Walder 1995). It is an X-ray source that falls in the class β of the X-ray sources amongst symbiotic stars: these are sources that show emission from an optically thin plasma with a temperature of a few 10^6 K (Mürset, Wolff & Jordan 1997).

The X-ray emission of the β-class sources is believed to originate from colliding stellar winds (CSW) in binary system (e.g., Mürset et al. 1997; Luna et al. 2013). Since a symbiotic binary consists of a red giant (possessing a massive but slow wind) and a white dwarf, that could well be the case provided the latter component has a stellar wind as well. This was exactly the case for AG Peg as shown by analysis of the Hubble Space Telescope spectra (Nussbaumer, Schmutz & Vogel 1995). However, the reported recent activity of AG Peg indicates that the physical picture in this old symbiotic nova might be more complicated than that.

In this work, our goal is to address the origin of the X-ray emission from the symbiotic star AG Peg by making use of the available X-ray data. In Section 2, we review the X-ray observations of AG Peg. In Section 3, we present results from analysis of the X-ray properties of AG Peg. In Section 4, we discuss the origin of the X-ray emission of this old symbiotic nova. Our conclusions are listed in Section 5.

2 X-RAY DATA

In this study, we used archive data of AG Peg from the X-ray observatories *ROSAT* and *Swift*.

ROSAT. We used one pointed observation taken on 1993 June 9 (ObsID rp300186n00). Following the recommendations for the *ROSAT* Data Processing[1], we extracted the source and background spectra. Since the data were

⋆ E-mail: szhekov@astro.bas.bg; toma.tomov@astri.umk.pl.

[1] http://heasarc.gsfc.nasa.gov/docs/rosat/rhp_proc_analysis.html

© 2016 The Authors

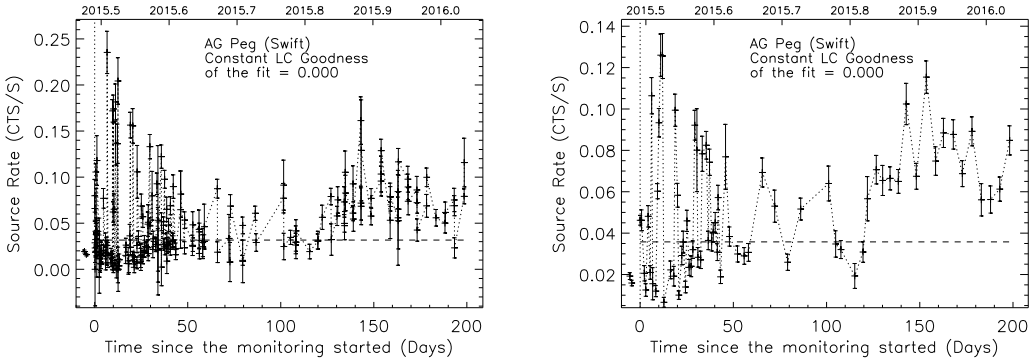

Figure 1. The (0.3 - 3 keV) background-subtracted light curves (LC) of AG Peg in 2015 (*Swift*). *Left* panel: the 'GTI' LC based on all the 71 observations. *Right* panel: the 'daily' LC based on the average count rate for each data set. The corresponding constant flux level is denoted by a dashed line. The count rates of both observations in 2013 are given for comparison at some fiducial negative time.

taken after 1991 Oct 14, we adopted the response matrix pspcb_gain2_256.rmf and we used the package *pcarf* to construct the ancillary response file. The extracted spectrum has 409 net source counts in an effective exposure of 5788 s.

Swift. We used 73 pointed observations (ObsID from 00032906001 to 00032906079; data sets with ObsID with the last two digits 17, 31, 38, 40, 49 and 51 do not exist in the archive) taken in 2013 August (two data sets) and in 2015 June - 2016 January (71 data sets). Following the *Swift* XRT Data Reduction Guide[2], we extracted the source and background spectra for each observation. Extraction regions had the same shape and size for each data set. For our analysis, we used the response matrix (swxpc0to12s6_20010101v014.rmf) provided by the most recent (2015 July 31) *Swift* calibration files[3] and we also used the package *xrtmkarf* to construct the ancillary response file for each data set. Due to the relatively short exposure times (e.g., between 200 and 9,000 s), the individual spectra have limited photon statistics in the (0.3 - 3 keV) energy band: the net source counts are between *even* less than 10 and ~ 300 ('typically' a few tens of counts). The total number of source counts in the entire sample of *Swift* spectra in 2015 is 6,440 (71 spectra) and 299 in 2013 (2 spectra). And, for those with more than 100 source counts (29 spectra), we have 4,586 net source counts in total.

For the spectral analysis in this study, we made use of standard as well as custom models in version 11.3.2 of XSPEC (Arnaud 1996).

3 RESULTS

The available data allows us to obtain some pieces of information on the X-ray properties of AG Peg: e.g., about its X-ray variability and the characteristics of its X-ray spectrum.

3.1 X-ray light curve

It is worth noting that the good time intervals (GTI) in the *Swift* observations of AG Peg are unevenly spaced. As a rule of thumb, the length of a GTI segment is shorter than the time 'gap' between two consecutive GTIs. This prevents constructing a 'standard' light curve (LC), that is a LC with equal time bins. For that reason, we constructed the following background-subtracted LCs: one, 'GTI' LC, that includes all the count rates from individual GTIs from all the observations in 2015 (195 GTIs in total) and another one, 'daily' LC, that includes all the average count rates for each data set (71 data sets). These LCs of AG Peg are shown in Fig. 1. Examples of the individual LCs (both from *Swift* and *ROSAT*), namely, those including only the GTIs for that specific date of observation, are shown in Appendix A (see Fig. A1).

To address the X-ray variability of AG Peg, we fitted a constant count rate model to the 'daily' as well as the 'GTI' LCs. The formal goodness of fit, using χ^2 fitting, is very small (equal to zero) for both LCs. This undoubtedly shows that AG Peg is a variable X-ray source on time scales of days: the *Swift* observations in 2015 span a time interval of $\sim$ 200 days. Applying the Lomb-Scargle method (Lomb 1976; Scargle 1982; see § 13.8 in Press et al. 1992), no periodicity was revealed in either of the X-ray LCs.

On the other hand, the individual LCs show both cases, that is of constant and variable flux, which means that variable X-ray emission on time scales of a few hours is not always present in AG Peg (note that only LCs with the goodness of the fit < 0.001 were assumed variable and such were $\sim 25\%$ of all the idividual LCs). However, due to the limited photon statistics of the *Swift* data on AG Peg caution is needed before drawing a firm conclusion. Future uninterrupted observations with higher sensitivity will be crucial to study the short-time (< 1 day) X-ray variability of this object.

3.2 X-ray spectrum

We recall that the *Swift* data on AG Peg have limited photon statistics (see Section 2). A standard way to analyse such data is to construct a total spectrum which could have

[2] http://swift.gsfc.nasa.gov/analysis/xrt_swguide_v1_2.pdf
[3] http://heasarc.gsfc.nasa.gov/docs/heasarc/caldb/swift/

Table 1. Spectral Model Results (*Swift*)

Model case	N_H	kT	norm	F_X	L_X
1T	0.69 (1.29)	0.59 (0.30)	1.67 (1.13) $\times 10^{-3}$	12.2 (7.0)	13.6 (9.5)
1T (N_H)	0.32	0.64 (0.35)	1.41 (0.83) $\times 10^{-3}$	12.2 (7.1)	11.4 (6.8)
1T (kT)	1.43 (1.10)	0.45	3.07 (2.06) $\times 10^{-3}$	12.2 (7.0)	19.8 (12.5)
1T (N_H, kT)	0.35	0.52	1.65 (0.97) $\times 10^{-3}$	12.0 (7.0)	11.7 (6.7)
CSW	1.58 (1.07)	...	3.22 (2.15)	12.3 (7.2)	23.3 (14.9)
CSW (N_H)	0.79	...	1.97 (1.13)	12.3 (7.0)	15.8 (9.1)

Note – Results from the fits to the *Swift* spectra of AG Peg. The '1T' and 'CSW' notations indicate the cases of one-temperature thin-plasma and colliding stellar wind models, respectively. The model parameter common (being the same) for all the spectra is given in parentheses therein. The model parameters are the X-ray absorption N_H in units of 10^{21} cm^{-2}, the plasma temperature kT in keV; the XSPEC model normalization (norm), the observed flux (0.3 - 3 keV energy range) F_X in units of 10^{-13} ergs cm^{-2} s^{-1} and luminosity in units of 10^{31} ergs s^{-1} for adopted distance of 800 pc (Kenyon et al. 1993, Kenyon et al. 2001). For each of them, given are the mean value followed in parentheses by the standard deviation for the entire sample of 73 spectra.

much higher quality. However, because of the high level of variability detected in the X-ray emission from this object (see Section 3.1), we instead analysed the individual spectra aimed at studying the global spectral properties of the X-ray emission from AG Peg and to address how they change in time.

Namely, we made use of the implementation of the Cash statistic (Cash 1979) in XSPEC for the model fits to the unbinned *Swift* spectra in the (0.3 - 3 keV) energy range. We note that the X-ray background is very low: its mean contribution in our sample of spectra is 4% of the total counts in extracted source spectra. Thus, we could simply neglect its contribution. Nevertheless, we constructed a common (total) background spectrum of all the *Swift* observations of AG Peg. A power-law model provided a very good fit to this total background spectrum, So, such a spectral component with fixed model parameters was used in the further fitting of the individual spectra.

3.2.1 Discrete-temperature models

Since AG Peg falls in the class β of the X-ray sources amongst symbiotic stars (showing emission form an optically thin plasma with a temperature of a few 10^6 K; Mürset et al. 1997), the adopted spectral model was a sum of an absorbed optically thin plasma emission and a background component, as explained above. For the H, He, C and N abundances, we adopted the values derived by Schmutz (1996): H : He : C : N = 1 : 0.1 : 10^{-5} : 10^{-3} by number (H = 1, He = 1.02, C = 0.03, N = 8.93 with respect to the solar abundances; Anders & Grevesse 1989). And to improve the quality of the fits, the O, Ne, Mg, Si and Fe abundances were allowed to vary. It is important to note that the spectral fitting was performed in two steps. First, we used only those spectra that have more than 100 X-ray counts. These spectra (29 in total) were fitted simultaneously allowing the O, Ne, Mg, Si and Fe abundances to vary. The derived abundance values (with 1σ errors) are: O = $0.67^{+0.05}_{-0.04}$, Ne = $0.00^{+0.02}_{-0.00}$, Mg = $0.02^{+0.05}_{-0.02}$, Si = $0.32^{+0.09}_{-0.05}$, Fe = $0.16^{+0.01}_{-0.01}$ (the values are with respect to the solar abundances; Anders & Grevesse 1989). Second, each individual spectrum was fitted with the same spectral model having abundance values fixed to those derived in the first step of the fitting. The free parameters for the individual fits were the amount of X-ray absorption, plasma temperature and normalization parameter.

Some fit results are shown in Figs. 2 and 3 as the formal goodness of the fit is very good for all the data sets. We note that there might be some trend in the change (increase) with time of the temperature of the X-ray emitting plasma as indicated by the results from the fit to the spectra with the better quality (X-ray counts higher than 100). The linear Pearson correlation coefficient is 0.83. Also, the X-ray absorption could be decreasing with time but the correlation is weak (the correlation coefficient is -0.38).

For completeness, we explored also the following cases of discrete-temperature models. We considered absorbed one-temperature thin-plasma emission as above but assuming that all the spectra were subject to the same X-ray absorption. Next, we adopted one-temperature plasma model but assuming that the plasma temperature was not changing with time. Finally, we considered the case where neither the X-ray absorption nor the plasma temperature were changing with time. In all these case, the spectral fits were performed following the same two-step procedure as explained above. We note that the quality of the fits was acceptable in all the cases under consideration, slightly decreasing with increasing the number of model parameters common for all the data sets: e.g., sharing the same X-ray absorption, or the same plasma temperature, or both.

Some basic results from the discrete-temperature model fits are summarized in Table 1. We see that it is safe to conclude that considerable variability of the basic parameters of the X-ray emission from AG Peg is present. This is valid for all the cases of absorbed one-temperature thin-plasma emission considered here. Namely, the value of the standard deviation for a given parameter is always more than 50% of the mean value of that model parameter for the sample of 73 *Swift* spectra at hand. This is indicative of a considerable scatter of that parameter, that is of its considerable variability with time. This conclusion is also supported by the large χ^2-value for the sample of derived values of a given parameter with respect of their associated mean, which results in a very small probability (equal to zero) for constancy of that parameter.

3.2.2 CSW model spectra

We recall that from the analysis of the *ROSAT* observation of AG Peg Mürset et al. (1995) proposed that the X-ray emission of this symbiotic star most likely originates

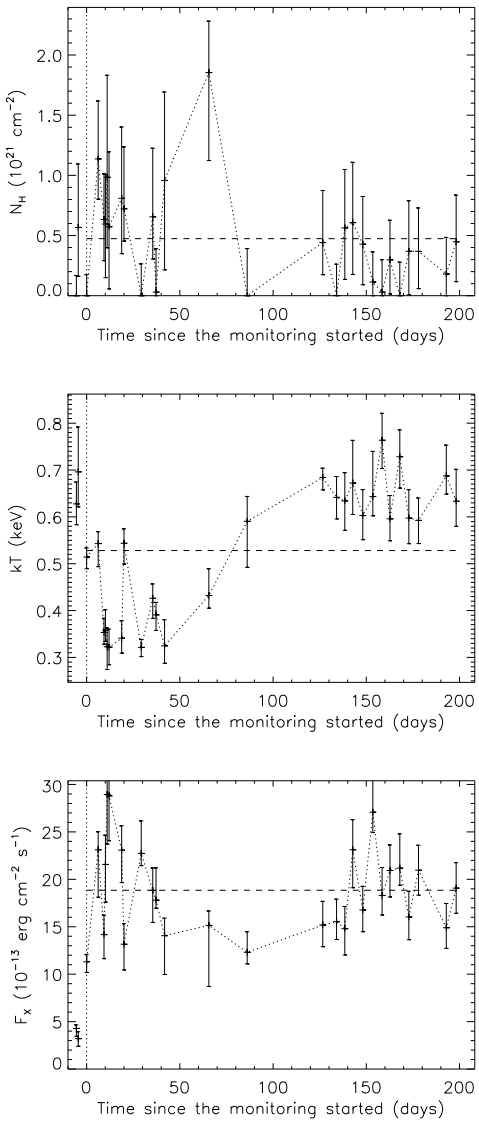
N_H (10^21 cm^-2)
Time since the monitoring started (days)
kT (keV)
Time since the monitoring started (days)
F_X (10^-13 erg cm^-2 s^-1)
Time since the monitoring started (days)

Figure 2. Results from the fits to the *Swift* spectra of AG Peg with optically thin plasma model for the data sets with higher than 100 X-ray counts. Shown are the time evolution of the X-ray absorption (N_H), plasma temperature (kT; 1 keV $= 11.6 \times 10^6$ K) and observed X-ray flux (0.3 - 3 keV). The horizontal dashed line indicates the mean value for the corresponding parameter. The results for both observations in 2013 are given at some fiducial negative time.

from colliding stellar winds. They also provided comparison of some physical quantities that were derived in hydrodynamic calculations with those deduced in the analysis of the *ROSAT* data. However, they did not provide a direct comparison of the theoretical and observed X-ray spectra. Here, we attempted such a direct comparison although in some approximate manner.

We note that the basic input parameters for the hydrodynamic model in CSW binaries are the mass loss and velocity of the stellar winds of the binary components and the binary separation. The former define a dimensionless parameter $\Lambda = (\dot{M}_{HS}V_{HS})/(\dot{M}_{CS}V_{CS})$ (the notations HS and CS stand for the hot star and cool star, respectively) which determines the shape and the structure of the CSW interaction region (Luo, McCray & Mac Low 1990; Stevens, Blondin & Pollock 1992; Myasnikov & Zhekov 1993). We adopted the same wind parameters as in Mürset et al. (1995): $\dot{M}_{HS} = 2 \times 10^{-7}$ M$_\odot$ yr^{-1}, $V_{HS} = 1000$ km s^{-1}, $\dot{M}_{CS} = 4 \times 10^{-7}$ M$_\odot$ yr^{-1}, $V_{CS} = 20$ km s^{-1}. For a binary period of 818.2 days (Fekel et al. 2000) and assuming a total binary mass of 2 solar masses, Kepler's third law gives a binary separation of 3.22×10^{13} cm.

It is worth noting that due to its high velocity only the shocked hot-star wind could be a source of X-ray emission. From the HS wind parameters, one sees that the shocked HS plasma will be adiabatic. This is indicated by the values of either of dimensionless parameters χ (Stevens et al. 1992) and Γ_{ff} (Myasnikov & Zhekov 1993): $\chi = 16.1$ ($\chi > 1$ - adiabatic case), $\Gamma_{ff} = 0.001$ ($\Gamma_{ff} > 1$ - cooling is important). In general, partial electron heating might occur behind strong shocks. However, the value of the dimensionless parameter $\Gamma_{eq} = 23.5$ indicates that the temperature equalization is very fast in the case of AG Peg ($\Gamma_{eq} < 1$ if the difference of electron and ion temperatures is important; see Zhekov & Skinner 2000). Also, the value of the dimensionless parameter $\Gamma_{NEI} = 12.72$ indicates that the non-equilibrium ionization effects (NEI) do not play an important role in the CSW region of AG Peg (the NEI effects must be taken into account if $\Gamma_{NEI} \leq 1$ but can be neglected if $\Gamma_{NEI} \gg 1$; see Zhekov 2007).

Finally, we note that the shocked cool-star plasma in the CSW region in AG Peg will not be adiabatic. But, due to the low CS wind velocity (that is, low shock velocity, correspondingly low plasma temperature) there will be no X-ray emission from the shock CS-wind plasma. Also, even if that part of the CSW region 'collapses' the shock surface will simply 'coincide' with that of the contact discontinuity (as the latter is calculated in the adiabatic case), which will cause no changes in the plasma distribution in the shocked HS-wind part of the CSW region.

In such an approximation, we ran a series of CSW models that consider plasma in collisional equilibrium ionization (CIE). We used the model by Zhekov (2007) that is based on the 2D hydrodynamic model of adiabatic CSWs by Myasnikov & Zhekov (1993). The latter assumes spherical symmetry of the stellar winds that have reached their terminal velocities before they collide. For the H, He, C and N abundances, we adopted the values derived by Schmutz (1996): H : He : C : N = 1 : 0.1 : 10^{-3} : 10^{-5} by number (H = 1, He = 1.02, C = 0.03, N = 8.93 with respect to the solar abundances; Anders & Grevesse 1989).

ROSAT. The CSW model with nominal stellar wind parameters matched well the shape of the observed spectrum. However, the theoretical flux (or emission measure) was 1.36 times higher than that observed. We recall that the X-ray luminosity (and flux) of the shocked plasma in the CSW region is $L_X \propto \dot{M}^2 V^{-3} a^{-1}$ (for the emission measure EM $\propto \dot{M}^2 V^{-2} a^{-1}$), where $\dot{M}$ is the stellar wind mass-loss, V is the wind velocity and a is the binary separation; see Luo et al. 1990; Myasnikov & Zhekov 1993). So, CSW model with slightly reduced mass-loss rates (0.86 of the nominal) was adopted.

Some CSW model fit results are given in Table 2

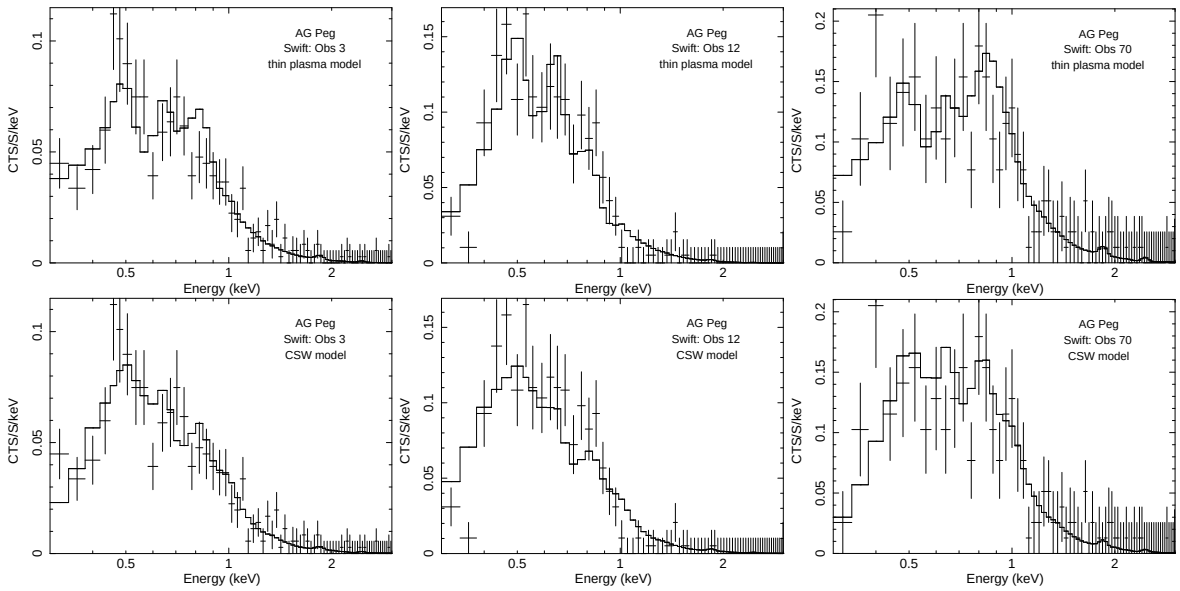

Figure 3. The *Swift* spectra of AG Peg that have more than 200 X-ray counts overlaid with the optically-thin plasma model fit (upper row) and with the CSW model fit for the case of CIE plasma (lower row). The spectra were slightly re-binned for presentation.

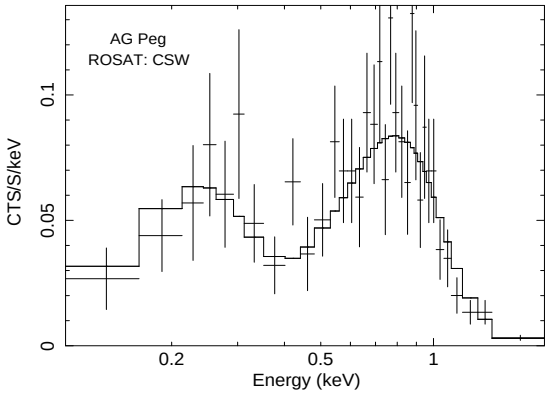

Figure 4. The background-subtracted spectrum of AG Peg from *ROSAT* with the CSW model fit for the case of CIE plasma. The spectrum was re-binned to have a minimum of 10 counts per bin.

and in Fig. 4. It is worth noting that the derived value of the hydrogen absorption column density translates into a range of optical extinction $A_V = 0.14 - 0.18$ mag. The range corresponds to the conversion that is used: $N_H = 2.22 \times 10^{21} A_V$ cm^{-2} (Gorenstein 1975). and $N_H = (1.6-1.7) \times 10^{21} A_V$ cm^{-2} (Vuong et al. 2003, Getman et al. 2005); So, we see no indication for any X-ray absorption in excess to the optical extinction to AG Peg ($E_{B-V} = 0.1 \pm 0.05$ mag; Kenyon et al. 1993; $E_{B-V} = 0.09 \pm 0.04$ mag; Vogel & Nussbaumer 1994).

Thus, it seems conclusive that the CSW model is capable of explaining the X-ray emission of AG Peg as observed with *ROSAT* in 1993 June.

Swift. It is then interesting to see whether the CSW model with nominal wind and binary parameters (see above) can match the X-ray emission from AG Peg as observed with *Swift* in 2013 and 2015. To do so, we adopted the same two-step approach as in the case of discrete-temperature models (Section 3.2.1).

Table 2. CSW Spectral Model Results (*ROSAT*)

Parameter	CIE
χ^2/dof	23/35
N_H (10^{21} cm^{-2})	$0.30^{+0.03}_{-0.03}$
norm	$1.00^{+0.07}_{-0.07}$
$F_{X,1}$ (10^{-13} ergs cm^{-2} s^{-1})	6.84 (11.0)
$F_{X,2}$ (10^{-13} ergs cm^{-2} s^{-1})	6.69 (8.15)

Note – Results from the fit to the *ROSAT* spectrum of AG Peg using model spectra from the CSW hydrodynamic simulations for the case with collisional ionization equilibrium (CIE). Tabulated quantities are the neutral hydrogen absorption column density (N_H), the normalization parameter (*norm*) and the absorbed X-ray flux ($F_{X,1}$ in the 0.1 - 2 keV energy range; $F_{X,2}$ in the 0.3 - 3 keV energy range) followed in parentheses by the unabsorbed value. The *norm* parameter is a dimensionless quantity that gives the ratio of the emission measure required by observations to that predicted by the model. A value of *norm* = 1.0 indicates a perfect match between both of them. The adopted abundances are those from Schmutz (1996). Errors are the 1σ values from the fit.

First, we fitted simultaneously those spectra that have more than 100 X-ray counts allowing the O, Ne, Mg, Si and Fe abundances to vary. The derived abundance values (with 1σ errors) are: O = $1.34^{+0.09}_{-0.12}$, Ne = $0.00^{+0.02}_{-0.00}$, Mg = $0.11^{+0.14}_{-0.11}$, Si = $0.55^{+0.18}_{-0.17}$, Fe = $0.55^{+0.05}_{-0.05}$ (the values are with respect to the solar abundances; Anders & Grevesse 1989). Second, each individual spectrum was fitted with the same CSW model having abundance values fixed to those derived in the first step. The free parameters for the individual fits were the amount of X-ray absorption and normalization parameter.

As in the case with discrete-temperature models (Section 3.2.1), the quality of the fits to individual spectra was very good and some fit results are shown in Figs. 5 and 3. It is worth noting that in the framework of the CSW model

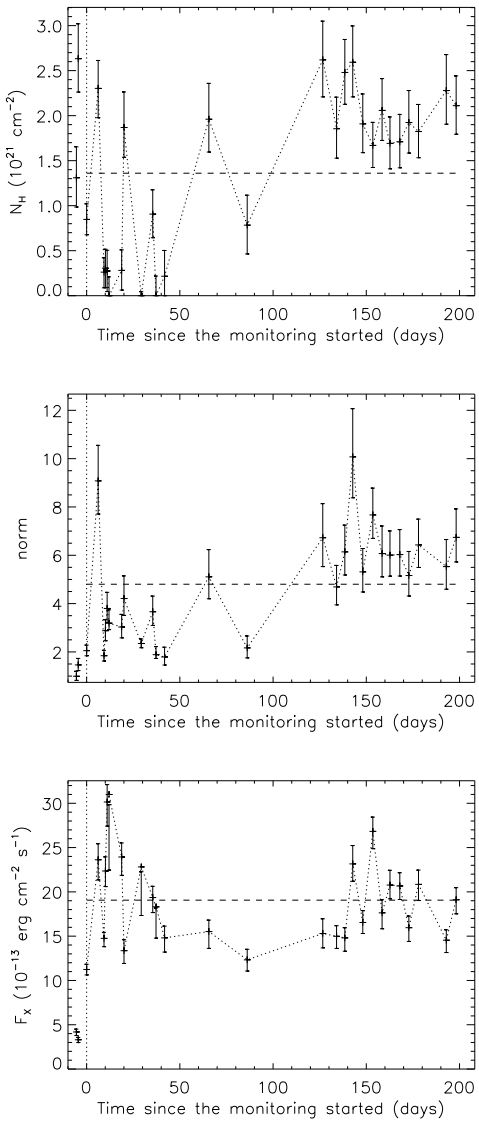
N_H (10^21 cm^-2)
Time since the monitoring started (days)
norm
Time since the monitoring started (days)
F_X (10^-13 erg cm^-2 s^-1)
Time since the monitoring started (days)

Figure 5. Results from the fits to the *Swift* spectra of AG Peg with the CSW model for the data sets with higher than 100 X-ray counts. Shown are the time evolution of the X-ray absorption (N_H), model normalization (norm) and observed X-ray flux (0.3 - 3 keV). The horizontal dashed line indicates the mean value for the corresponding parameter. The results for both observations in 2013 are given at some fiducial negative time.

these results suggest that the amount of shocked plasma in 2013 was about the same as in 1993 (*ROSAT* observation). However, it has increased considerably in 2015 and not only that but it varies on relatively short time scale (days). This follows from the values of the normalization parameter (*norm*) which is proportional to the emission measure of the hot plasma. Such changes require changes in the mass-loss rates at least by a factor of 2 ($norm \propto \dot{M}^2$; see above and also Zhekov 2007 for details). As in the case of discrete-temperature models, the amount of X-ray absorption varies considerably with time.

Following the approach adopted in the discrete-temperature model fitting, we considered the case of CSW model with common (being the same) X-ray absorption for all the data set. This is equivalent to having no variability of the X-ray absorption with time. We note that the quality of the fits in this case was acceptable as well although lower than in the standard CSW model case discussed above. Some fit results are given in Table 1 which also illustrate the considerable variability of the amount of shocked plasma needed to explain the observed variability in the X-ray emission of AG Peg. We will return to these results in Section 4.

4 ORIGIN OF THE X-RAY EMISSION

Our analysis of the *Swift* data on AG Peg showed that its X-ray spectrum can be presented by emission from an optically thin plasma with a temperature of a few 10^6 K (Section 3.2.1; Fig. 2). This means that AG Peg is of the class β of the X-ray sources amongst symbiotic stars as proposed by Mürset et al. (1997). But, probably the most important result from the *Swift* observations is the considerable X-ray variability that is present on time scales of days (and in some cases even hours; Section 3.1; Fig. 1; Appendix A).

We recall that Mürset et al. (1995) suggested that the X-ray emission from AG Peg is related to colliding stellar winds in binary system. In this study, we showed that the *ROSAT* spectrum (1993 June) of AG Peg can well be presented by X-ray emission from CSWs in binary system. The adopted values of the stellar wind and orbital parameters in the CSW model correspond to those deduced from analysis in other spectral domains (e.g., Schmutz 1996; Fekel et al. 2000).

On the other hand, the X-ray emission from AG Peg in 2013 and 2015 (*Swift*) does not seem to originate from CSWs. The most solid argument against the validity of the CSW picture in this case is the considerable X-ray variability that is present on time scales smaller than the CSW dynamical time in AG Peg ($t_{dyn} = a/V = 3.7$ days; a is the binary separation and V is the wind velocity), i.e. on time scales of a couple of days (and in some cases even hours). This requires appreciable changes of the mass-loss rates by 20-50% and even by a factor of 2 on the same time scale. Similarly, considerable changes of the X-ray absorption are deduced from analysis of the *Swift* spectra in 2015 as indicated by Figure 5 and Table 1. The difference in X-ray absorption on the *point-by-point* basis is at the $(2-4)\sigma$ level with respect to zero ('identical' N_H values), especially, in the first 40 days (July to mid-August 2015; the average time interval between the data points is 1.1 days) after the *Swift* monitoring has started. We note that such X-ray absorption changes are hard to expect in the framework of the CSW picture. It is so since the CSW region is a 3D object with a size at least as large as the size ot the binary orbit (> 2 au in AG Peg). So, to 'hide' such a large structure and/or dissolve the 'curtains' (increase and/or decrease the X-ray absorption) on time scales of days does not seem realistic. Namely, the physical agent that causes such changes on a dynamical time of a day should have a bulk velocity higher than 3,000 km s^{-1} (> 2 au / 86,400 s). So, such fast changes could indicate a size of the X-ray emission region *much smaller* than that of the CSW region in AG Peg. Another characteristic of the X-ray light curves of AG Peg might be also pointing in that direction.

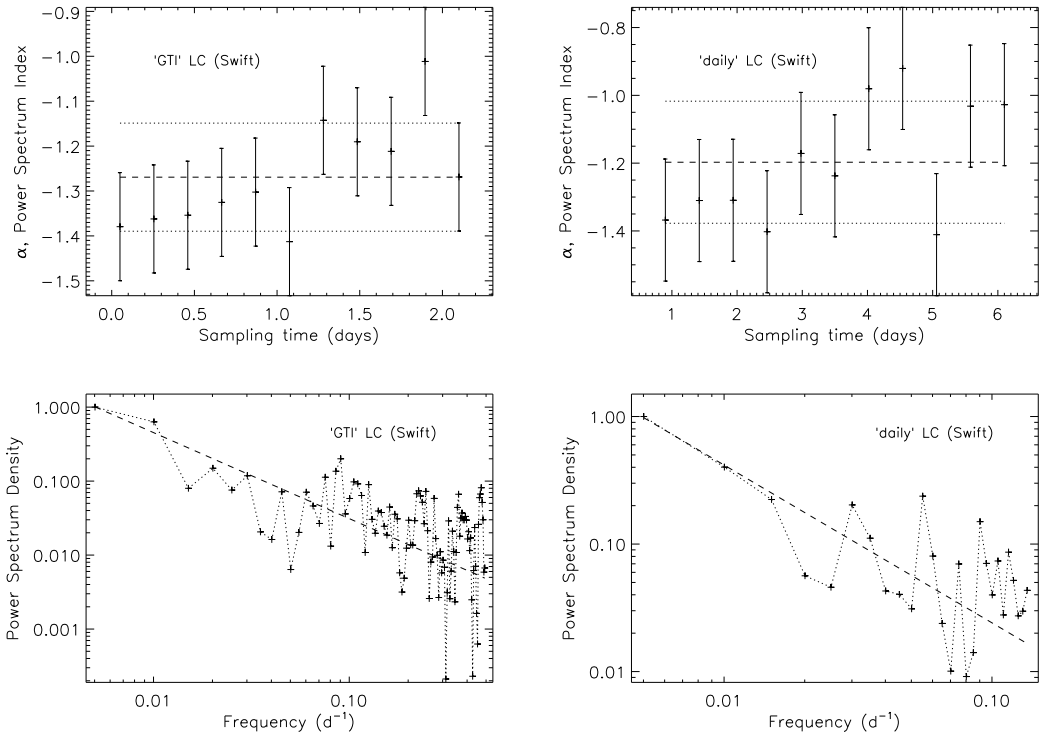

Figure 6. *Upper panels.* The power-law index derived from the fits with a power-law function to the power spectrum (PS) of the X-ray LCs (PS $\propto f^{\alpha}$, $f = 1$/time). The mean value for the results with different sampling time of the LC is shown by a dashed line. The dotted lines mark its 1σ (standard deviation) confidence interval. *Lower panels.* Examples of the model fits (dashed line) to the power spectrum (in log scale) for the cases with the respective mean value of the sampling-time ranges (1 day for the 'GTI' LC, $\alpha = -1.16 \pm 0.06$; 3.5 days for the 'daily' LC, $\alpha = -1.24 \pm 0.10$). The PS is normalized to its maximum value for presentation.

Namely, we tried to estimate the power spectrum of the X-ray LCs obtained in the *Swift* observations of AG Peg.

We recall that the data points in the *Swift* LCs ('daily' LC and 'GTI' LC) are not equidistant in time (see Section 3.1). For the power spectrum of a LC, we thus used a linear interpolation to 'project' the LC onto a grid with equal time step. Then, we made use of the FFT (Fast Fourier Transform) algorithm to calculate the power spectrum (PS). Finally, we fitted a power-law function to the resultant power spectrum of the LC under consideration: PS $\propto f^{\alpha}$, $f = 1$/time. Interestingly, the fitted power-law index had negative values: $\alpha \approx -1$. To check how this result depends on the sampling time of the LC, we explored a range for the time bins of the resultant 'equidistant' LC. This range was chosen trying to avoid 'extreme' oversampling of the original LC as well as to avoid having just few data points in the resultant one. Namely, the range covers about 70-75% of the number of time steps (intervals) in the original LCs as only the 10-15% of the shortest and of the longest time steps were excluded. The corresponding fit results are (mean value followed by the standard deviation in parentheses; Fig. 6): $\alpha = -1.20$ (0.18) for the 'daily' LC; $\alpha = -1.27$ (0.12) for the 'GTI' LC.

In order to test this result, we adopted the following approach. We simulated a LC that has a power spectrum with the same α-value as derived for the observed LC. A normal (Gaussian) noise was added too. The simulated LC covers a time interval from a few hundreds to more than a thousand days. Using the time grid of the observed LC and a randomly chosen LC start time, we extracted a large number (e.g., a thousand) of 'theoretical' LCs. Each of these were processed exactly in the same manner as the observed LC. The result was that the derived values of α were about normally distributed with mean value very close to that of the observed LC, in fact, within one standard deviation. This numerical test gave us additional confidence in the derived α-values of the power spectrum of the X-ray LCs of AG Peg.

It is interesting to note that the values of α derived from the X-ray variability of AG Peg are close to $\alpha = -1$ which is characteristic of the so called flicker noise (or flickering) found in many astronomical objects and typical for variety of physical phenomena (e.g., see Press 1978). In astronomical objects, flickering is usually found in systems that harbour degenerate objects like black holes, neutron stars, white dwarfs and is related to accretion processes. Then, the power spectrum of the LCs of AG Peg as observed with *Swift* in 2015 might be also indicating that the X-rays in this symbiotic system do not originate in CSWs.

Thus, to explain the observed X-ray properties of AG Peg in 1993-2013-2015, we could assume that (a) CSWs did play a key role in generating the X-ray emission in 1993 (*ROSAT*); (b) in the period before 2013, AG Peg switched to a different mode, that is, the stellar wind of the hot component (a white dwarf; WD) has seized and the accretion of the cool star wind onto the WD started. We recall that such a change in AG Peg has been suggested earlier (see

Zamanov & Tomov 1995 for details). However, if this were indeed the case, some 'drastic' changes in the optical spectrum of AG Peg should have occurred as well. Among others, there must be no signs of *strong* stellar wind from the hot component in this symbiotic binary. Interestingly, this is exactly what is found by Tomov, Stoyanov & Zamanov (2016, MNRAS, submitted) from the analysis of optical emission of AG Peg as observed in 2015. These authors suggest that a new phase in the evolution of AG Peg is under way, which finds further support from the analysis of the *Swift* data on this object presented here.

However, it is important to note that the *Swift* spectra of AG Peg do not manifest signs of highly absorbed and strong emission at high energies (above 2.4 keV). Such kind of emission is considered typical for the so called δ and β/δ X-ray sources among the symbiotic stars and is assumed to originate in the accretion-disk boundary layer (Luna et al. 2013).

One reason for not detecting X-ray emission at high energies could be purely technical: the really short exposure times of the *Swift* spectra of AG Peg.

To explore this a bit more, we created a total spectrum by summing up all the 71 spectra in 2015. The total spectrum shows that some weak emission is present in the 2 - 5 keV energy range. A thin-plasma model with at least two temperature components ($kT_{low} \sim 0.5$ keV; $kT_{high} \sim 2.7$ keV) could match that high-energy emission. But, we emphasize it again that this exercise had purely technical meaning since it is not advisable (e.g., in physical sense the result might be misleading) to create a total spectrum for a source exhibiting high variability with appreciable spectral changes as is the case of AG Peg (see Fig. 1 and Table 1). The latter is the most likely explanation why the quality of the fit to the total spectrum using the two-temperature model was not high ($\chi^2/dof = 150/96$). Thus, *individual* X-ray spectra with good quality are needed to reveal if high energy X-ray emission is present in this object and to constrain its characteristics.

But as mentioned above, another reason for the lack of high energy X-ray emission could be related to the actual physical processes taking plays in AG Peg.

We recall that thermal emission with relatively low plasma temperatures ($kT \leq 1$ keV) is considered a sign of CSWs in the symbiotic stars. But, an important ingredient is mandatory to have this mechanism working. Namely, it is the presence of relatively strong and fast stellar wind from the hot component, which is established from observations in other spectral domains (UV, optical). Such was indeed present around the time of the *ROSAT* spectrum of AG Peg (Nussbaumer et al. 1995; Schmutz 1996). However, analysis by Tomov et al. (2016) of recent optical spectra of AG Peg showed that no such wind is present any more.

But, let us consider the results from the optical (Tomov et al. 2016) in a conservative way. Namely, had they *only* meant that the stellar wind of the hot component in AG Peg is now considerably less massive (i.e. harder to detect), the X-ray emission from the supposed CSW region in the system could have been substantially reduced (see the scaling law for CSWs discussed in Section 3.2.2). Therefore, we would expect weaker X-ray emission in recent observations. Opposite to this, the X-ray emission from AG Peg has increased considerably compared to its level of about two decades ago. Thus even adopting a conservative approach, additional component is needed to describe the observed X-ray properties of AG Peg. Moreover, keeping in mind that the considerable X-ray variability of AG Peg is very hard to accommodate in the framework of a plausible (= not too speculative) CSW picture and that its time characteristics resemble those of a flicker noise (flickering), it is our understanding that a different process is getting into play and accretion onto a degenerate hot companion seems the most likely to us.

Additional support for the probable importance of accretion processes in AG Peg comes from its UV light curve. We note that analysis of the complete set of UV observations of AG Peg with *Swift* is beyond the scope of this work: in detail analysis is postponed to another paper. Here, we only mention the results for the data set with the longest exposure (Obs 3; 2015 June 28; the observation identification is the same as for the X-ray data; see Section 2). Namely, the UV light curve of Obs 3 clearly shows appreciable variability on time scales of minutes and hours (Appendix B; Fig.B1). Such a UV variability is quite typical for the δ X-ray sources among the symbiotic stars for which accretion is assumed to play an important role (see section 5.2 in Luna et al. 2013).

Finally, since AG Peg is likely in transition to a new evolutionary phase (from a symbiotic nova to a classical symbiotic star; Tomov et al. 2016), it might well be that it does not exactly match any specific case in the classification scheme by Luna et al. (2013) of the X-ray sources among the symbiotic stars. On the one hand, most of the X-ray emission of AG Peg is at energies below 2 keV, thus, resembling a β X-ray source. On the other hand, strong variability is present, thus, resembling sources fuelled by accretion processes. Also, the average X-ray luminosity of AG Peg ($L_X > 10^{32}$ egrs s^{-1}; Table 1) seems typical for a δ X-ray source (see section 5.2 in Luna et al. 2013), thus, again indicating likely importance of accretion processes. We believe that further X-ray observations of AG Peg will be very helpful to follow the evolution of its properties and to finally settle its classification status as X-ray source among the symbiotic stars.

5 CONCLUSIONS

In this work, we analysed archive X-ray data (*ROSAT* and *Swift*) on the symbiotic binary AG Peg. The basic results and conclusions are as follows.

(i) The X-ray emission of AG Peg as observed with *Swift* in 2015 shows considerable variability on time scale of days as variability on shorter time scales might be present as well. No periodicity is present in the available data (2015 June - 2016 January).

(ii) Analysis of the X-ray spectra obtained in 2013 and 2015 confirms that AG Peg is an X-ray source of class β of the X-ray sources amongst the symbiotic stars. That is, its X-ray spectrum can be presented by emission from an optically thin plasma with a temperature of a few 10^6 K.

(iii) The X-ray emission of AG Peg as observed with *ROSAT* (1993 June) might well originate from colliding stellar winds in binary system. The CSW model with values that correspond to the stellar wind and orbital parameters deduced from analysis in other spectral domains (e.g.,

Schmutz 1996; Fekel et al. 2000) can match very well the *ROSAT* spectrum of AG Peg.

(iv) On the other hand, the characteristics of the X-ray emission of AG Peg as observed with *Swift* in 2013 and 2015 are hard to accommodate in the framework of the CSW picture. Namely, such are the considerable changes of the amount of X-ray emitting plasma and the X-ray absorption on time scale of one-two days.

(v) Analysis of the *Swift* light curves in 2015 shows that the power spectrum of the X-ray variability in AG Peg can be matched by a power-law function, PS $\propto f^{\alpha}$, $f = 1/\text{time}$, with $\alpha \approx -1.2$. This value is close to $\alpha = -1$, which is characteristic of the flicker noise (or flickering) being typical for accretion processes in astronomical objects. This, along with the result mentioned above in (iv), is a sign that CSWs did not play a key role for the X-ray emission from AG Peg as observed in 2013-2015 and a different mechanism (probably accretion) is likely getting into play.

(vi) Further monitoring of the X-ray emission from AG Peg will be very helpful to reveal *in detail* the physical picture in this fascinating symbiotic star. Also, uninterrupted X-ray observations with good quality will be very important to show whether the flickering is present on short time scales (< 1 day).

ACKNOWLEDGEMENTS

This research has made use of data and/or software provided by the High Energy Astrophysics Science Archive Research Center (HEASARC), which is a service of the Astrophysics Science Division at NASA/GSFC and the High Energy Astrophysics Division of the Smithsonian Astrophysical Observatory. This research has made use of the NASA's Astrophysics Data System, and the SIMBAD astronomical data base, operated by CDS at Strasbourg, France. The authors thank an anonymous referee for some comments and suggestions.

REFERENCES

Anders E., Grevesse N., 1989, Geochimica Cosmochimica Acta, 53, 197
Arnaud K. A., 1996, in Jacoby G. H., Barnes J., eds, Astronomical Society of the Pacific Conference Series Vol. 101, Astronomical Data Analysis Software and Systems. p. 17
Cash W., 1979, ApJ, 228, 939
Fekel F. C., Joyce R. R., Hinkle K. H., Skrutskie M. F., 2000, AJ, 119, 1375
Getman K. V., Feigelson E. D., Grosso N., McCaughrean M. J., Micela G., Broos P., Garmire G., Townsley L., 2005, ApJS, 160, 353
Gorenstein P., 1975, ApJ, 198, 95
Kenyon S. J., Mikolajewska J., Mikolajewski M., Polidan R. S., Slovak M. H., 1993, AJ, 106, 1573
Kenyon S. J., Proga D., Keyes C. D., 2001, AJ, 122, 349
Lomb N. R., 1976, Ap&SS, 39, 447
Luna G. J. M., Sokoloski J. L., Mukai K., Nelson T., 2013, A&A, 559, A6
Luna G. J. M., Nunez E. N., Sokoloski L. J., Montane B., 2015, The Astronomer's Telegram, 7741
Luo D., McCray R., Mac Low M.-M., 1990, ApJ, 362, 267
Munari U., Valisa P., Dallaporta S., Cherini G., Righetti G. L., Castellani F., 2013, The Astronomer's Telegram, 5258
Mürset U., Jordan S., Walder R., 1995, A&A, 297, L87
Mürset U., Wolff B., Jordan S., 1997, A&A, 319, 201
Myasnikov A. V., Zhekov S. A., 1993, MNRAS, 260, 221
Nunez E. N., Luna M. G. J., 2013, The Astronomer's Telegram, 5324
Nussbaumer H., Schmutz W., Vogel M., 1995, A&A, 293, L13
Press W. H., 1978, Comments on Astrophysics, 7, 103
Press W. H., Teukolsky S. A., Vetterling W. T., Flannery B. P., 1992, Numerical recipes in FORTRAN. The art of scientific computing. Cambridge: University Press, |c1992, 2nd ed.
Ramsay G., Luna G. J. M., Nunez E. N., Sokoloski L. J., Montane B., 2015, The Astronomer's Telegram, 7779
Scargle J. D., 1982, ApJ, 263, 835
Schmutz W., 1996, in Benvenuti P., Macchetto F. D., Schreier E. J., eds, Science with the Hubble Space Telescope - II. p. 366
Stevens I. R., Blondin J. M., Pollock A. M. T., 1992, ApJ, 386, 265
Vogel M., Nussbaumer H., 1994, A&A, 284, 145
Vuong M. H., Montmerle T., Grosso N., Feigelson E. D., Verstraete L., Ozawa H., 2003, A&A, 408, 581
Zamanov R. K., Tomov N. A., 1995, The Observatory, 115, 185
Zhekov S. A., 2007, MNRAS, 382, 886
Zhekov S. A., Skinner S. L., 2000, ApJ, 538, 808

APPENDIX A: INDIVIDUAL X-RAY LIGHT CURVES OF AG Peg

Here, we show a sample of the individual *background-subtracted* light curves of AG Peg in the (0.3 - 3 keV) energy range, based on the good time intervals in the *ROSAT* and *Swift* observations (see Section 3.1). To address the X-ray variability, we fitted a constant count rate model to each individual LC using χ^2 fitting. The formal goodness of fit is given in each plot (Fig. A1). The 2015 *Swift* light curves were chosen to have at least 3 data points and to be representative of the short time variability over the entire observation period (2015 June - 2016 January).

APPENDIX B: UV SHORT TIME SCALE VARIABILITY OF AG Peg

The Ultraviolet/Optical Telescope (UVOT) aboard *Swift* allows for obtaining UV data on a given target simultaneously with its X-ray data. This was the case for all the *Swift* observations of AG Peg discussed in this work (see Section 2). Here, we show some results for Obs 3 (ObsID 00032906003) taken on 2015 June 28. On this date, UVOT observed AG Peg in the UVM2 filter ($\lambda_0 = 2231$ Å, FWHM = 498 Å) taking 11 different exposures (good time intervals; GTI) in image mode. Following the Swift UVOT Data Reduction Guide[4], we analysed the corresponding event data file for each GTI. We filtered the event file in time domain that allowed us to build the corresponding short time scale light curves by making use of the *uvotevtlc* script. We considered only those GTIs with exposures longer than 300 s (9 in total for Obs 3). The resultant UV LCs are shown in Fig. B1. We see that on 2015 June 28 appreciable variability of 0.05 - 0.1 mag was definitely present in the UV emission of AG Peg on time scales of minutes and hours.

[4] http://swift.gsfc.nasa.gov/analysis/UVOT_swguide_v2_2.pdf

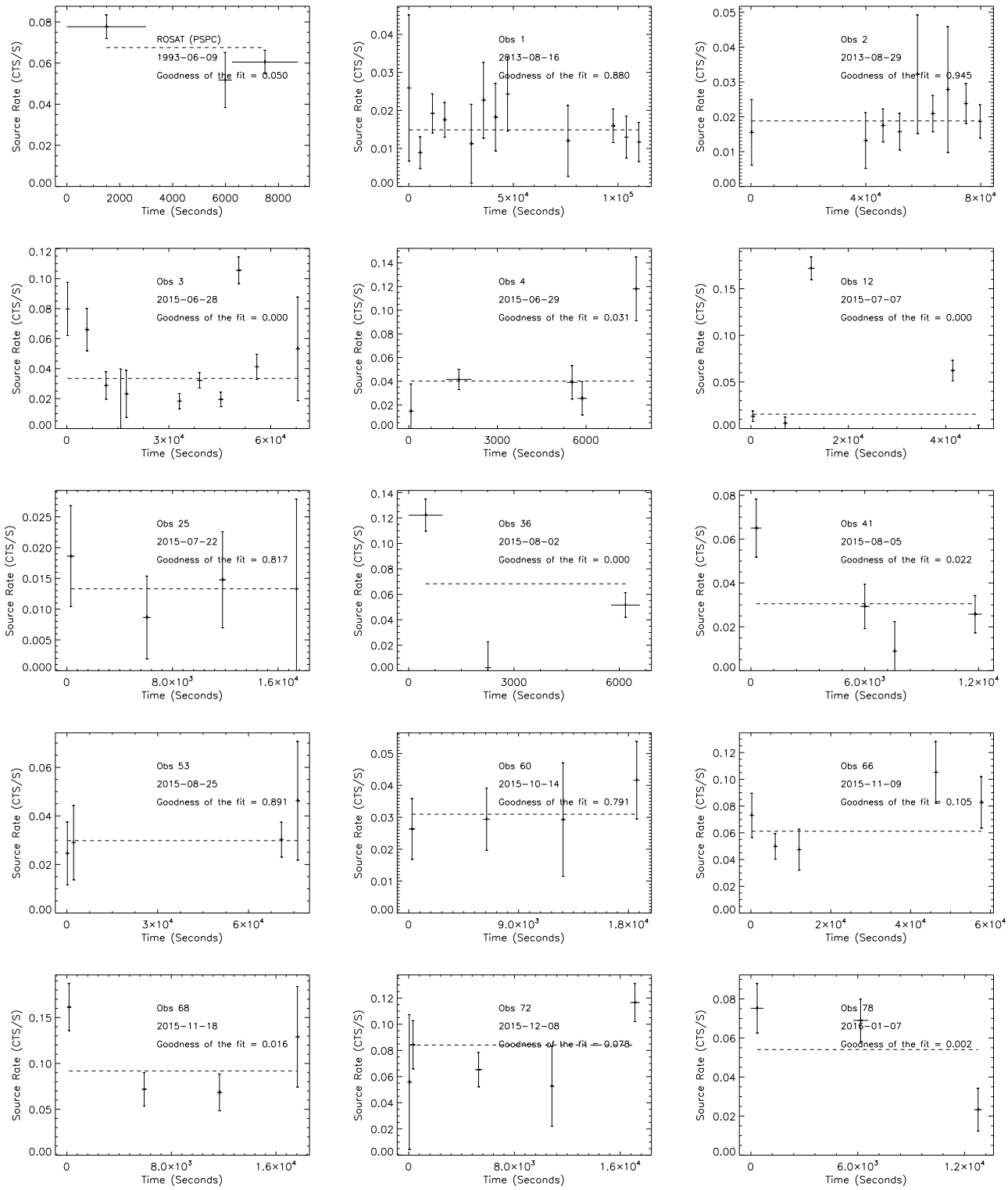

Figure A1. The AG Peg individual light curves (*ROSAT* and *Swift*). The corresponding constant flux level is denoted by a dashed line. The horizontal bar gives the time bin for each data point. The observation number corresponds to the last two digits in the *Swift* ObsID (see Section 2).

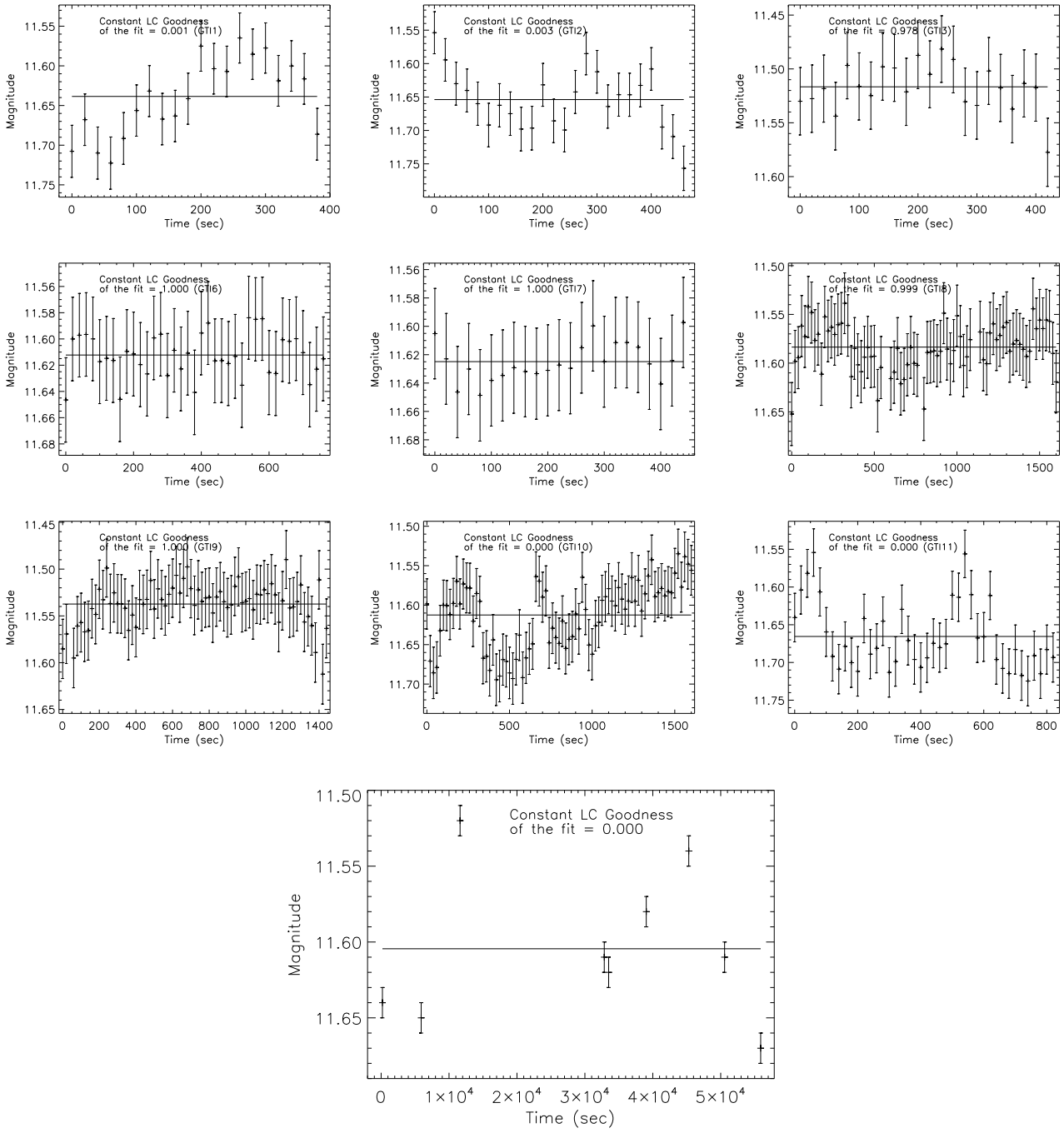
Constant LC Goodness of the fit = 0.001 (GTI1)
Constant LC Goodness of the fit = 0.003 (GTI2)
Constant LC Goodness of the fit = 0.978 (GTI5)
Constant LC Goodness of the fit = 1.000 (GTI6)
Constant LC Goodness of the fit = 1.000 (GTI7)
Constant LC Goodness of the fit = 0.999 (GTI8)
Constant LC Goodness of the fit = 1.000 (GTI9)
Constant LC Goodness of the fit = 0.000 (GTI10)
Constant LC Goodness of the fit = 0.000 (GTI11)
Constant LC Goodness of the fit = 0.000
Magnitude
Time (sec)

Figure B1. The UVOT light curves (time bins of 20 s) of AG Peg in the UVM2 filter for the *Swift* observation on 2015 June 28. The corresponding constant magnitude level is denoted by a dashed line. The consecutive GTI number is denoted in each panel. The total LC (GTI-average) is shown in the bottom panel.

This paper has been typeset from a TEX/LATEX file prepared by the author.